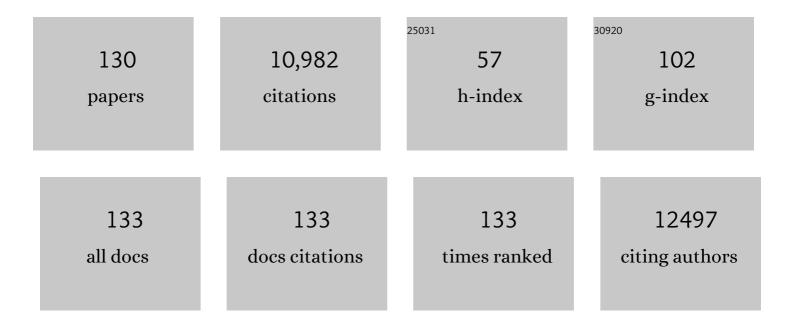
List of Publications by Year in descending order

Source: https://exaly.com/author-pdf/4560889/publications.pdf Version: 2024-02-01



CHISHENC LL

#	Article	IF	CITATIONS
1	Photocatalytic fuel cell – A review. Chemical Engineering Journal, 2022, 428, 131074.	12.7	57
2	Photoelectrocatalytic Reduction of CO <sub>2</sub> to Syngas via SnO <i><sub>x</sub></i> â€Enhanced Cu <sub>2</sub> O Nanowires Photocathodes. Advanced Functional Materials, 2022, 32, 2109600.	14.9	42
3	Microwaveâ€Positioning Assembly: Structure and Surface Optimizations for Catalysts. Small Structures, 2022, 3, .	12.0	6
4	Dual-emitting metal–organic frameworks for ratiometric fluorescence detection of fluoride and Al3+ in sequence. Spectrochimica Acta - Part A: Molecular and Biomolecular Spectroscopy, 2022, 271, 120896.	3.9	15
5	Polarization field promoted photoelectrocatalysis for synergistic environmental remediation and H2 production. Chemical Engineering Journal, 2022, 437, 135132.	12.7	20
6	Carbon Nanotube-Threaded Mesocrystalline CeO <sub>2</sub> for Enhanced Photocatalytic NO Removal. ACS Applied Nano Materials, 2022, 5, 3581-3590.	5.0	12
7	Fullerene–Graphene Acceptor Drives Ultrafast Carrier Dynamics for Sustainable CdS Photocatalytic Hydrogen Evolution. Advanced Functional Materials, 2022, 32, .	14.9	55
8	Complete mineralization of phenolic compounds in visible-light-driven photocatalytic ozonation with single-crystal WO3 nanosheets: Performance and mechanism investigation. Journal of Hazardous Materials, 2022, 433, 128811.	12.4	18
9	Microwave-assisted synthesis of oxygen vacancy associated TiO2 for efficient photocatalytic nitrate reduction. Chinese Chemical Letters, 2022, 33, 3835-3841.	9.0	25
10	Singlet Oxygen and Mobile Hydroxyl Radicals Co-operating on Gas–Solid Catalytic Reaction Interfaces for Deeply Oxidizing NO <sub><i>x</i></sub> . Environmental Science & Technology, 2022, 56, 5830-5839.	10.0	22
11	Rutile TiO2 nanorods grown on carbon nanotubes as high-performance lithium-ion batteries anode via one-dimensional electron pathways. Journal of Sol-Gel Science and Technology, 2022, 103, 437-446.	2.4	3
12	Femtosecond time-resolved spectroscopic observation of long-lived charge separation in bimetallic sulfide/g-C3N4 for boosting photocatalytic H2 evolution. Applied Catalysis B: Environmental, 2021, 282, 119568.	20.2	97
13	Porous g-C <sub>3</sub> N <sub>4</sub> /TiO <sub>2</sub> foam photocatalytic filter for treating NO indoor gas. Environmental Science: Nano, 2021, 8, 1571-1579.	4.3	10
14	Photo-induced dye-sensitized BiPO4/BiOCl system for stably treating persistent organic pollutants. Applied Catalysis B: Environmental, 2021, 285, 119841.	20.2	73
15	Research Progress on Photocatalytic/Photoelectrocatalytic Oxidation of Nitrogen Oxides. Transactions of Tianjin University, 2021, 27, 295.	6.4	9
16	CO2 reduction to formic acid via NH2-C@Cu2O photocatalyst in situ derived from amino modified Cu-MOF. Journal of CO2 Utilization, 2021, 54, 101781.	6.8	22
17	Horizontally arranged zinc platelet electrodeposits modulated by fluorinated covalent organic framework film for high-rate and durable aqueous zinc ion batteries. Nature Communications, 2021, 12, 6606.	12.8	369
18	Visible-light-driven hydrogen peroxide production from water and dioxygen by perylenetetracarboxylic diimide modified titanium-based metal–organic frameworks. Journal of Materials Chemistry A, 2021, 9, 26371-26380.	10.3	38

#	Article	IF	CITATIONS
19	Acute and repeated dose 26-week oral toxicity study of 20(S)-ginsenoside Rg3 in Kunming mice and Sprague–Dawley rats. Journal of Ginseng Research, 2020, 44, 222-228.	5.7	28
20	3D-Printed Grids with Polymeric Photocatalytic System as Flexible Air Filter. Applied Catalysis B: Environmental, 2020, 262, 118307.	20.2	28
21	Repeated-dose 26-week oral toxicity study of ginsenoside compound K in Beagle dogs. Journal of Ethnopharmacology, 2020, 248, 112323.	4.1	9
22	A 26-week 20(S)-ginsenoside Rg3 oral toxicity study in Beagle dogs. Regulatory Toxicology and Pharmacology, 2020, 110, 104522.	2.7	12
23	Cooperation between inside and outside of TiO2: Lattice Cu+ accelerates carrier migration to the surface of metal copper for photocatalytic CO2 reduction. Applied Catalysis B: Environmental, 2020, 264, 118515.	20.2	93
24	Efficient Self-Driving Photoelectrocatalytic Reactor for Synergistic Water Purification and H <sub>2</sub> Evolution. ACS Applied Materials & Interfaces, 2020, 12, 44731-44742.	8.0	33
25	A strong hydrangea-like Au–TiO <sub>2</sub> catalyst for round-the-clock degradation of oxalic acid in the presence of ozone. Catalysis Science and Technology, 2020, 10, 7481-7485.	4.1	5
26	Self-Suspended Photothermal Microreactor for Water Desalination and Integrated Volatile Organic Compound Removal. ACS Applied Materials & amp; Interfaces, 2020, 12, 51537-51545.	8.0	47
27	MOFs Conferred with Transient Metal Centers for Enhanced Photocatalytic Activity. Angewandte Chemie - International Edition, 2020, 59, 17182-17186.	13.8	121
28	NH2-UiO-66(Zr) with fast electron transfer routes for breaking down nitric oxide via photocatalysis. Applied Catalysis B: Environmental, 2020, 267, 118687.	20.2	83
29	Photoanode driven photoelectrocatalytic system for CO2 reduction to formic acid by using CoOx cathode. Applied Surface Science, 2020, 511, 145497.	6.1	24
30	In-situ fabrication SnO2/SnS2 heterostructure for boosting the photocatalytic degradation of pollutants. Chinese Journal of Catalysis, 2020, 41, 1554-1563.	14.0	24
31	Gas-Phase Photoelectrocatalytic Oxidation of NO <i>via</i> TiO <sub>2</sub> Nanorod Array/FTO Photoanodes. Environmental Science & Technology, 2020, 54, 5902-5912.	10.0	42
32	Microwave-induced Assembly of CuS@MoS <sub>2</sub> Core-shell Nanotubes and Study on Their Photocatalytic Fenton-like Reactions. Acta Chimica Sinica, 2020, 78, 961.	1.4	12
33	Strong Hollow Spherical La <sub>2</sub> NiO <sub>4</sub> Photocatalytic Microreactor for Round-the-Clock Environmental Remediation. ACS Applied Materials & Interfaces, 2019, 11, 25967-25975.	8.0	33
34	Edgeâ€Enriched Ultrathin MoS <sub>2</sub> Embedded Yolkâ€Shell TiO <sub>2</sub> with Boosted Charge Transfer for Superior Photocatalytic H <sub>2</sub> Evolution. Advanced Functional Materials, 2019, 29, 1901958.	14.9	115
35	A flexible CdS nanorods-carbon nanotubes/stainless steel mesh photoanode for boosted photoelectrocatalytic hydrogen evolution. Chemical Communications, 2019, 55, 2741-2744.	4.1	48
36	TiO2 nanotube arrays modified with nanoparticles of platinum group metals (Pt, Pd, Ru): enhancement on photoelectrochemical performance. Journal of Nanoparticle Research, 2019, 21, 1.	1.9	24

#	Article	IF	CITATIONS
37	Probing supramolecular assembly and charge carrier dynamics toward enhanced photocatalytic hydrogen evolution in 2D graphitic carbon nitride nanosheets. Applied Catalysis B: Environmental, 2019, 256, 117867.	20.2	137
38	Preclinical safety of ginsenoside compound K: Acute, and 26-week oral toxicity studies in mice and rats. Food and Chemical Toxicology, 2019, 131, 110578.	3.6	29
39	Highly Selective and Efficient Synthesis of 7-Aminoquinolines and Their Applications as Golgi-Localized Probes. ACS Medicinal Chemistry Letters, 2019, 10, 954-959.	2.8	40
40	Photocatalysis: Microwaveâ€Induced Metal Dissolution Synthesis of Core–Shell Copper Nanowires/ZnS for Visible Light Photocatalytic H <sub>2</sub> Evolution (Adv. Energy Mater. 22/2019). Advanced Energy Materials, 2019, 9, 1970085.	19.5	2
41	Gas-Phase Photoelectrocatalysis for Breaking Down Nitric Oxide. Environmental Science & Technology, 2019, 53, 7145-7154.	10.0	45
42	Microwaveâ€Induced Metal Dissolution Synthesis of Core–Shell Copper Nanowires/ZnS for Visible Light Photocatalytic H <sub>2</sub> Evolution. Advanced Energy Materials, 2019, 9, 1900775.	19.5	97
43	Copper Phosphide-Enhanced Lower Charge Trapping Occurrence in Graphitic-C <sub>3</sub> N <sub>4</sub> for Efficient Noble-Metal-Free Photocatalytic H <sub>2</sub> Evolution. ACS Applied Materials & Interfaces, 2019, 11, 16527-16537.	8.0	83
44	A chloroplast structured photocatalyst enabled by microwave synthesis. Nature Communications, 2019, 10, 1570.	12.8	88
45	Imine-bridged periodic mesoporous organosilica as stable high-activity catalytic for Knoevenagel reaction in aqueous medium. Research on Chemical Intermediates, 2019, 45, 3107-3121.	2.7	7
46	Efficient Photocatalytic Fuel Cell via Simultaneous Visible-Photoelectrocatalytic Degradation and Electricity Generation on a Porous Coral-like WO <sub>3</sub> /W Photoelectrode. Environmental Science & Technology, 2019, 53, 3697-3706.	10.0	105
47	Interfacial optimization of g-C3N4-based Z-scheme heterojunction toward synergistic enhancement of solar-driven photocatalytic oxygen evolution. Applied Catalysis B: Environmental, 2019, 244, 240-249.	20.2	295
48	g-C3N4 photoanode for photoelectrocatalytic synergistic pollutant degradation and hydrogen evolution. Applied Surface Science, 2019, 467-468, 658-665.	6.1	82
49	Microwave irradiation induced UIO-66-NH2 anchored on graphene with high activity for photocatalytic reduction of CO2. Applied Catalysis B: Environmental, 2018, 228, 47-53.	20.2	186
50	Thermally stable TiO2 quantum dots embedded in SiO2 foams: Characterization and photocatalytic H2 evolution activity. Applied Catalysis B: Environmental, 2018, 229, 130-138.	20.2	62
51	MICROSTRUCTURE AND PROPERTIES OF THE Ni–B AND Ni–B–Ce ULTRASONIC-ASSISTED ELECTROLESS COATINGS. Surface Review and Letters, 2018, 25, 1950006.	1.1	6
52	Controllable synthesis of mesoporous multi-shelled ZnO microspheres as efficient photocatalysts for NO oxidation. Applied Surface Science, 2018, 435, 468-475.	6.1	47
53	Nanotube Array-Like WO <sub>3</sub> Photoanode with Dual-Layer Oxygen-Evolution Cocatalysts for Photoelectrocatalytic Overall Water Splitting. ACS Applied Energy Materials, 2018, 1, 6871-6880.	5.1	60
54	Aerosol-Assisted Synthesis of Spherical Sb/C Composites as Advanced Anodes for Lithium Ion and Sodium Ion Batteries. ACS Applied Energy Materials, 2018, 1, 6381-6387.	5.1	32

#	Article	IF	CITATIONS
55	Graphene oxide enhanced amine-functionalized titanium metal organic framework for visible-light-driven photocatalytic oxidation of gaseous pollutants. Applied Catalysis B: Environmental, 2018, 236, 501-508.	20.2	116
56	Photoelectrocatalytic reduction of CO 2 to methanol over a photosystem II-enhanced Cu foam/Si-nanowire system. Journal of Environmental Sciences, 2017, 60, 108-113.	6.1	19
57	Mesoporous single-crystal-like TiO2 mesocages threaded with carbon nanotubes for high-performance electrochemical energy storage. Nano Energy, 2017, 35, 44-51.	16.0	75
58	Genotoxicity testing of sodium formononetin-3′-sulphonate (Sul-F) by assessing bacterial reverse mutation, chromosomal aberrations and micronucleus tests. Regulatory Toxicology and Pharmacology, 2017, 86, 374-378.	2.7	7
59	Nonclinical safety of astilbin: A 4-week oral toxicity study in rats with genotoxicity, chromosomal aberration, and mammalian micronucleus tests. Food and Chemical Toxicology, 2017, 107, 1-9.	3.6	21
60	Controlling charge transfer in quantum-size titania for photocatalytic applications. Applied Catalysis B: Environmental, 2017, 215, 85-92.	20.2	52
61	Pt-Enhanced Mesoporous Ti <sup>3+</sup> /TiO <sub>2</sub> with Rapid Bulk to Surface Electron Transfer for Photocatalytic Hydrogen Evolution. ACS Applied Materials & Interfaces, 2017, 9, 16959-16966.	8.0	147
62	Acute and a 28-day repeated-dose toxicity study of total flavonoids from Clinopodium chinense (Benth.) O. Ktze in mice and rats. Regulatory Toxicology and Pharmacology, 2017, 91, 117-123.	2.7	14
63	Nanotube array-like WO3/W photoanode fabricated by electrochemical anodization for photoelectrocatalytic overall water splitting. Chinese Journal of Catalysis, 2017, 38, 2132-2140.	14.0	37
64	A 90-day subchronic toxicity study with sodium formononetin-3′-sulphonate (Sul-F) delivered to dogs via intravenous administration. Regulatory Toxicology and Pharmacology, 2016, 77, 87-92.	2.7	16
65	Hollow spherical RuO 2 @TiO 2 @Pt bifunctional photocatalyst for coupled H 2 production and pollutant degradation. Applied Catalysis B: Environmental, 2016, 194, 42-49.	20.2	130
66	Porous CuO nanotubes/graphene with sandwich architecture as high-performance anodes for lithium-ion batteries. Nanoscale, 2016, 8, 19343-19351.	5.6	48
67	Nanotube-confinement induced size-controllable g-C3N4 quantum dots modified single-crystalline TiO2 nanotube arrays for stable synergetic photoelectrocatalysis. Nano Energy, 2016, 19, 446-454.	16.0	329
68	Microwave-antenna induced in situ synthesis of Cu nanowire threaded ZIF-8 with enhanced catalytic activity in H <sub>2</sub> production. Nanoscale, 2016, 8, 7749-7754.	5.6	32
69	Photoelectrocatalytic hydrogen generation and simultaneous degradation of organic pollutant via CdSe/TiO2 nanotube arrays. Applied Surface Science, 2016, 362, 490-497.	6.1	85
70	CNTs threaded (001) exposed TiO <sub>2</sub> with high activity in photocatalytic NO oxidation. Nanoscale, 2016, 8, 2899-2907.	5.6	50
71	Microwave-assisted synthesis of Ag-doped MOFs-like organotitanium polymer with high activity in visible-light driven photocatalytic NO oxidization. Applied Catalysis B: Environmental, 2015, 172-173, 46-51.	20.2	98
72	Uniform anatase single-crystal cubes with high thermal stability fully enclosed by active {010} and {001} facets. RSC Advances, 2015, 5, 11029-11035.	3.6	12

#	Article	IF	CITATIONS
73	C <sub>60</sub> -Decorated CdS/TiO <sub>2</sub> Mesoporous Architectures with Enhanced Photostability and Photocatalytic Activity for H <sub>2</sub> Evolution. ACS Applied Materials & Interfaces, 2015, 7, 4533-4540.	8.0	148
74	Ag2O/TiO2 nanorods heterojunctions as a strong visible-light photocatalyst for phenol treatment. Journal of Sol-Gel Science and Technology, 2015, 73, 314-321.	2.4	22
75	Plasmonic silver quantum dots coupled with hierarchical TiO2 nanotube arrays photoelectrodes for efficient visible-light photoelectrocatalytic hydrogen evolution. Scientific Reports, 2015, 5, 10461.	3.3	113
76	Synthesis of Ce ions doped metal–organic framework for promoting catalytic H <sub>2</sub> production from ammonia borane under visible light irradiation. Journal of Materials Chemistry A, 2015, 3, 14134-14141.	10.3	102
77	Copper Nanowires: A Substitute for Noble Metals to Enhance Photocatalytic H <sub>2</sub> Generation. Nano Letters, 2015, 15, 4853-4858.	9.1	111
78	The self-assembly synthesis of tungsten oxide quantum dots with enhanced optical properties. Journal of Materials Chemistry C, 2015, 3, 3280-3285.	5.5	74
79	Highly Efficient and Stable Au/CeO <sub>2</sub> –TiO <sub>2</sub> Photocatalyst for Nitric Oxide Abatement: Potential Application in Flue Gas Treatment. Langmuir, 2015, 31, 10822-10830.	3.5	69
80	Hierarchical Nanostructured WO <sub>3</sub> with Biomimetic Proton Channels and Mixed Ionic-Electronic Conductivity for Electrochemical Energy Storage. Nano Letters, 2015, 15, 6802-6808.	9.1	157
81	Ionothermal synthesis of black Ti <sup>3+</sup> -doped single-crystal TiO <sub>2</sub> as an active photocatalyst for pollutant degradation and H <sub>2</sub> generation. Journal of Materials Chemistry A, 2015, 3, 3748-3756.	10.3	141
82	Plasmon-induced photoelectrocatalytic activity of Au nanoparticles enhanced TiO2 nanotube arrays electrodes for environmental remediation. Applied Catalysis B: Environmental, 2015, 164, 217-224.	20.2	182
83	Synergy effect in photodegradation of contaminants from water using ordered mesoporous carbon-based titania catalyst. Applied Catalysis B: Environmental, 2014, 146, 151-161.	20.2	35
84	An efficient dye-sensitized BiOCl photocatalyst for air and water purification under visible light irradiation. Environmental Sciences: Processes and Impacts, 2014, 16, 1975-1980.	3.5	66
85	Vertically aligned CdTe nanotube arrays on indium tin oxide for visible-light-driven photoelectrocatalysis. Applied Catalysis B: Environmental, 2014, 147, 17-21.	20.2	20
86	Au nanoparticles enhanced rutile TiO2 nanorod bundles with high visible-light photocatalytic performance for NO oxidation. Applied Catalysis B: Environmental, 2014, 147, 610-616.	20.2	119
87	C <sub>60</sub> /Bi <sub>2</sub> TiO <sub>4</sub> F <sub>2</sub> Heterojunction Photocatalysts with Enhanced Visible-Light Activity for Environmental Remediation. ACS Applied Materials & Interfaces, 2013, 5, 7190-7197.	8.0	72
88	Photoelectrocatalytic degradation of organic pollutants via a CdS quantum dots enhanced TiO2 nanotube array electrode under visible light irradiation. Nanoscale, 2013, 5, 2118.	5.6	205
89	Improvement of the Visibleâ€Light Photocatalytic Performance of TiO <sub>2</sub> by Carbon Mesostructures. Chemistry - A European Journal, 2013, 19, 566-577.	3.3	56
90	Core-shell structure CdS/TiO2 for enhanced visible-light-driven photocatalytic organic pollutants degradation. Journal of Sol-Gel Science and Technology, 2013, 66, 504-511.	2.4	29

#	Article	IF	CITATIONS
91	Mesoporous TiN Microspheres with Hierarchical Chambers and Enhanced Visible Lightâ€Driven Hydrogen Evolution. ChemSusChem, 2013, 6, 1461-1466.	6.8	26
92	The Development of Better Photocatalysts through Composition―and Structureâ€Engineering. Chemistry - an Asian Journal, 2013, 8, 26-40.	3.3	71
93	Environmental Photocatalysis 2013. International Journal of Photoenergy, 2013, 2013, 1-3.	2.5	4
94	An efficient round-the-clock La2NiO4 catalyst for breaking down phenolic pollutants. RSC Advances, 2012, 2, 4822.	3.6	25
95	Self-assembled 3D architectures of Bi2TiO4F2 as a new durable visible-light photocatalyst. Nanoscale, 2012, 4, 455-460.	5.6	47
96	WO3 nanocrystals with tunable percentage of (001)-facet exposure. Applied Catalysis B: Environmental, 2012, 123-124, 398-404.	20.2	76
97	Synthesis of Ultralong Copper Nanowires for High-Performance Transparent Electrodes. Journal of the American Chemical Society, 2012, 134, 14283-14286.	13.7	366
98	A novel nanoreactor framework of iodine-incorporated BiOCl core–shell structure: enhanced light-harvesting system for photocatalysis. CrystEngComm, 2012, 14, 700-707.	2.6	84
99	Microwave-Induced Synthesis of Porous Single-Crystal-Like TiO <sub>2</sub> with Excellent Lithium Storage Properties. Langmuir, 2012, 28, 4543-4547.	3.5	52
100	Microwave-assisted architectural control fabrication of 3D CdS structures. Journal of Sol-Gel Science and Technology, 2012, 62, 140-148.	2.4	10
101	Ethanol supercritical route for fabricating bimodal carbon modified mesoporous TiO2 with enhanced photocatalytic capability in degrading phenol. Applied Catalysis B: Environmental, 2012, 115-116, 236-244.	20.2	51
102	Ionothermal synthesis of hierarchical BiOBr microspheres for water treatment. Journal of Hazardous Materials, 2012, 211-212, 104-111.	12.4	126
103	Photocatalytic destruction of air pollutants with vacuum ultraviolet (VUV) irradiation. Catalysis Today, 2011, 175, 310-315.	4.4	59
104	Graphite-like carbon deposited anatase TiO2 single crystals as efficient visible-light photocatalysts. Journal of Sol-Gel Science and Technology, 2011, 58, 594-601.	2.4	23
105	Template-free synthesis of hierarchical porous SnO2. Journal of Sol-Gel Science and Technology, 2010, 53, 499-503.	2.4	8
106	Monosteps on the Surfaces of Mesostructured Silica and Titania Thin Films. Small, 2010, 6, 1880-1885.	10.0	6
107	Green synthesis of a self-assembled rutile mesocrystalline photocatalyst. CrystEngComm, 2010, 12, 1759.	2.6	84
108	Design, Fabrication, and Modification of Nanostructured Semiconductor Materials for Environmental and Energy Applications. Langmuir, 2010, 26, 3031-3039.	3.5	464

GUISHENG LI

#	Article	IF	CITATIONS
109	Biocompatible Anatase Single-Crystal Photocatalysts with Tunable Percentage of Reactive Facets. Crystal Growth and Design, 2010, 10, 1130-1137.	3.0	120
110	An Efficient Bismuth Tungstate Visible-Light-Driven Photocatalyst for Breaking Down Nitric Oxide. Environmental Science & Technology, 2010, 44, 4276-4281.	10.0	170
111	Inorganic materials for photocatalytic water disinfection. Journal of Materials Chemistry, 2010, 20, 4529.	6.7	173
112	Mesoporous Ni–B amorphous alloy microspheres with tunable chamber structure and enhanced hydrogenation activity. Chemical Communications, 2010, 46, 791-793.	4.1	48
113	A mesoporous TiO2â^'xNx photocatalyst prepared by sonication pretreatment and in situ pyrolysis. Separation and Purification Technology, 2009, 67, 152-157.	7.9	24
114	Synthesis of Size-Tunable Monodispersed Metallic Nickel Nanocrystals without Hot Injection. Crystal Growth and Design, 2009, 9, 2812-2815.	3.0	31
115	A micrometer-size TiO2 single-crystal photocatalyst with remarkable 80% level of reactive facets. Chemical Communications, 2009, , 4381.	4.1	327
116	Thermally stable ordered mesoporous CeO2/TiO2 visible-light photocatalysts. Physical Chemistry Chemical Physics, 2009, 11, 3775.	2.8	152
117	Aerosol-spraying synthesis of SiO2/TiO2 nanocomposites and conversion to porous TiO2 and single-crystalline TiOF2. Chemical Communications, 2009, , 5394.	4.1	59
118	A Meaningful Analogue of Pentacene: Charge Transport, Polymorphs, and Electronic Structures of Dihydrodiazapentacene. Chemistry of Materials, 2009, 21, 1400-1405.	6.7	63
119	Direct encoding of silica submicrospheres with cadmium telluride nanocrystals. Journal of Materials Chemistry, 2009, 19, 7002.	6.7	20
120	Ordered Mesoporous BiVO <sub>4</sub> through Nanocasting: A Superior Visible Light-Driven Photocatalyst. Chemistry of Materials, 2008, 20, 3983-3992.	6.7	340
121	Effect of Carbon Doping on the Mesoporous Structure of Nanocrystalline Titanium Dioxide and Its Solar-Light-Driven Photocatalytic Degradation of NO <i><sub>x</sub></i> . Langmuir, 2008, 24, 3510-3516.	3.5	288
122	Synthesis of silver nanowire/mesoporous silica composite as a highly active antiseptic. Studies in Surface Science and Catalysis, 2007, , 841-846.	1.5	4
123	Mesoporous Titania Spheres with Tunable Chamber Stucture and Enhanced Photocatalytic Activity. Journal of the American Chemical Society, 2007, 129, 8406-8407.	13.7	1,119
124	An active La/TiO2 photocatalyst prepared by ultrasonication-assisted sol–gel method followed by treatment under supercritical conditions. Journal of Molecular Catalysis A, 2007, 278, 237-243.	4.8	91
125	Hierarchical mesoporous grape-like titania with superior recyclability and photoactivity. Microporous and Mesoporous Materials, 2007, 106, 278-283.	4.4	24
126	An ordered cubic Im3m mesoporous Cr–TiO2visible light photocatalyst. Chemical Communications, 2006, , 2717-2719.	4.1	117

#	Article	IF	CITATIONS
127	Preparation of an active SO42â°/TiO2 photocatalyst for phenol degradation under supercritical conditions. Journal of Molecular Catalysis A, 2005, 226, 93-100.	4.8	77
128	Carbon/graphite seal materials prepared from mesocarbon microbeads. Carbon, 2004, 42, 1427-1433.	10.3	50
129	An Effective TiO2Photocatalyst Prepared under Supercritical Conditions. Chemistry Letters, 2004, 33, 574-575.	1.3	12
130	rGO uO <sub>x</sub> Composites Reduced by Solidâ€Phase Microwave Thermal Shock for Highâ€Efficient Seawater Desalination and Purification. Advanced Sustainable Systems, 0, , 2100500.	5.3	3